X. X. Chen

P. D. Wu[1]
e-mail: peidong@mcmaster.ca

Department of Mechanical Engineering,
McMaster University,
Hamilton, ON, L8S 4L7, Canada

D. J. Lloyd
Novelis Global Technology Centre,
945 Princess Street,
Kingston, ON, K7L 5L9, Canada

J. D. Embury
Department of Materials Science and Engineering,
McMaster University,
Hamilton, ON, L8S 4L7, Canada

Y. Huang
Department of Civil and Environmental Engineering and Department of Mechanical Engineering,
Northwestern University,
Evanston, IL 60208

Enhanced Ductility in Sheet Metals Produced by Cladding a Ductile Layer

The effect of cladding a ductile layer on necking and fracture in sheet metals under plane strain tension is studied numerically using the finite element method based on the Gurson damage model. It is demonstrated that the cladding increases both the necking and fracture strains. The increase in necking strain is due to the fact that cladding a ductile layer enhances the overall work hardening for the layered metal sheets according to the rule of mixtures. Furthermore, the increase in necking strain slows down the development of the triaxial tensile stress inside the neck, which delays the void nucleation and growth, and which, in turn, contributes to enhancement in ductility. [DOI: 10.1115/1.4000926]

Keywords: fracture, necking, damage criteria, finite element, laminated

1 Introduction

Laminated composites consist of alternating material layers that are bonded with sharp interfaces. Laminated metal sheets produced by cladding different alloy combinations have been used for many years in the aerospace industry. Traditional products are "compromised" monolithic materials designed to meet the requirements of physical, mechanical, chemical, and surface properties, formability, and cost. Cladding/laminating decouples these requirements to enable new materials to be developed using alloys optimized for their function in the composite. Lesuer et al. [1] comprehensively reviewed mechanical behavior of laminated structures. In general, laminated composites can dramatically improve many properties including fracture toughness [2], fatigue behavior [3], and impact behavior [4], or provide enhanced formability or ductility [5–7].

Cladding sheets are generally produced by roll bonding [8,9], where the clad layer is bonded to the core by rolling at elevated temperatures. This adds considerably to the cost of the sheet since the clad layer is produced via scalping, preheating, rolling, and trimming with an additional surface preparation step prior to bonding, as well as "tacking" or strapping the clad to the scalped core prior to preheating and rolling. There are also issues with the alloy combinations that can be roll bonded, since some alloys form tenacious oxide films that are difficult to disrupt during the bonding process. This can result in low strength, dirty interfaces that degrade the useful strength of sheet. Recently developed Novelis Fusion Technology simultaneously casts multiple alloy layers into a single aluminum rolling ingot [10]. Novelis Fusion Technology produces a high quality ingot with a core of one aluminum alloy, combined with one or more layers of different aluminum alloys. The ingot can then be rolled into a sheet product with different properties on the inside and outside, allowing previously unattainable performance for flat rolled products and creating opportunities for new, premium applications. It is therefore expected that more and more clad sheet metals will be used in the manufacturing industry. This means that a comprehensive scientific program to understand the metallurgy and mechanics of the potential clad systems and to optimize clad alloys combinations must be pursued.

The purpose of this paper is to carry out a detailed numerical study of the influence of cladding a ductile soft layer on fracture in sheet metals under plane strain tension. All simulations reported in the present paper are performed using ABAQUS and the mechanical behavior of the sheet metals are characterized by the Gurson damage model [11,12].

2 Constitutive Model

All simulations reported in the present study will be based on the damage model originally developed by Gurson [11] and later modified by Tvergaard [13,14], and Tvergaard and Needleman [15]. In this section, we very briefly recap the constitutive model; for details, we refer to Ref. [12].

Assume that $\boldsymbol{\sigma}$ is the macroscopic Cauchy stress tensor and $\bar{\sigma}$ is the matrix flow strength. The approximate yield function for a porous plastic solid with a randomly distributed volume fraction f of voids is presented in the form of

$$\phi(\boldsymbol{\sigma},\bar{\sigma},f)=\frac{\sigma_e^{\,2}}{\bar{\sigma}^2}+2f^*q_1\cosh\left(\frac{3q_2\sigma_H}{2\bar{\sigma}}\right)-[1+(q_2f^*)^2]=0 \quad (1)$$

where σ_e and σ_H are the effective and mean stresses, respectively. The parameters q_1 and q_2 are calibration coefficients introduced by Tvergaard [13] to improve the agreement with numerical studies of materials containing periodically distributed circular, cylindrical, or spherical voids. The function $f^*(f)$ was introduced by

[1]Corresponding author.

Contributed by the Applied Mechanics Division of ASME for publication in the JOURNAL OF APPLIED MECHANICS. Manuscript received July 22, 2009; final manuscript received October 1, 2009; published online April 16, 2010. Editor: Robert M. McMeeking.

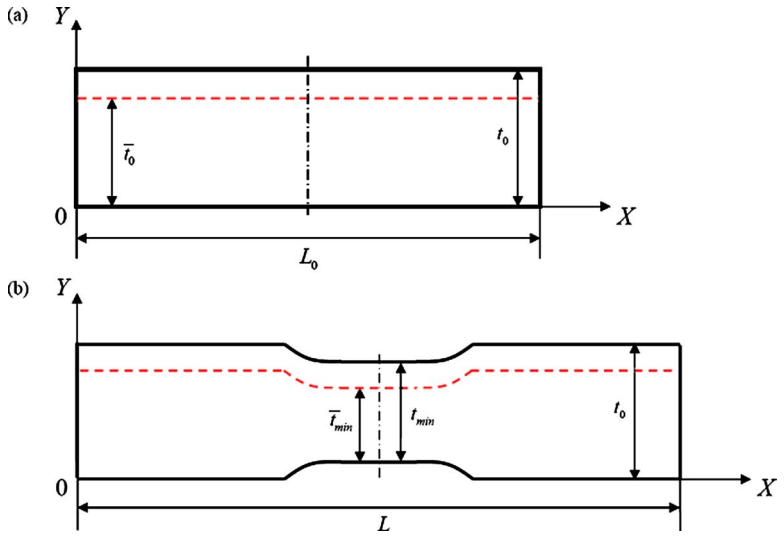

Fig. 1 Schematic representation of a tensile sheet with a ductile cladding layer: (*a*) initial and (*b*) deformed states

Tvergaard and Needleman [15] to model the loss of stress carrying capacity accompanying void coalescence, such that

$$f^* = \begin{cases} f & \text{for } f \le f_c \\ f_c + \dfrac{f_u^* - f_c}{f_f - f_c}(f - f_c) & \text{for } f > f_c \end{cases} \tag{2}$$

where f_c is the porosity level at which void coalescence commences and f_f is the porosity level at the final fracture. The parameter $f_u^* = 1/q_1$ is defined so that when $f = f_f$ the material has experienced a complete loss of strength. The evolution of void volume fraction is due to the growth of existing voids and the nucleation of new voids

$$\dot{f} = (\dot{f})_{\text{growth}} + (\dot{f})_{\text{nucleation}} \tag{3}$$

with the growth being a function of the plastic strain rate $\boldsymbol{D}^p$

$$(\dot{f})_{\text{growth}} = (1 - f)\boldsymbol{I}:\boldsymbol{D}^p \tag{4}$$

and the nucleation according to

$$(\dot{f})_{\text{nucleation}} = \bar{A}\dot{\bar{\varepsilon}}^p \tag{5}$$

where $\dot{\bar{\varepsilon}}^p$ is the effective plastic strain rate, and the parameter $\bar{A}$ is chosen so that nucleation follows a normal distribution, as suggested by Chu and Needleman [16]

$$\bar{A} = \frac{f_N}{s_N\sqrt{2\pi}} \exp\left[-\frac{1}{2}\left(\frac{\bar{\varepsilon}^p - \varepsilon_N}{s_N} \right)^2 \right] \tag{6}$$

where ε_N is the average void nucleating strain, f_N is the volume fraction of void nucleating particles, and s_N is the standard deviation of void nucleating strain. The original Gurson model has been improved significantly [17–19].

The uniaxial true stress-true strain curve for the matrix material is described by the following power-law form:

$$\bar{\varepsilon} = \begin{cases} \dfrac{\bar{\sigma}}{E} & \text{for } \bar{\sigma} \le \sigma_y \\ \dfrac{\sigma_y}{E}\left(\dfrac{\bar{\sigma}}{\sigma_y} \right)^n & \text{for } \bar{\sigma} > \sigma_y \end{cases} \tag{7}$$

where σ_y is the yield stress and n is the strain hardening exponent.

3 Problem Formulation and Method of Solution

Consider a metal sheet with initial length L_0 and initial thickness t_0, as shown in Fig. 1(*a*). It is assumed that the sheet consists of a core, with thickness $\bar{t}_0$, and a soft cladding layer, with thickness $(t_0 - \bar{t}_0)$. The cladding thickness ratio Γ is thus defined as $\Gamma = (t_0 - \bar{t}_0)/t_0$. Based on the work reported in Ref. [10], the cladding layer and core are assumed to be perfectly bonded.

We assume that the sheet is very wide and no deformation in the width direction, i.e., the sheet is under in-plane plane strain tension. The boundary conditions imposed on the sheet are

$$\begin{aligned} &\dot{u}_x = -\dot{U}, \quad \dot{u}_y = 0, \quad X = 0 \\ &\dot{u}_x = +\dot{U}, \quad \dot{u}_y = 0, \quad X = L_0 \end{aligned} \tag{8}$$

The tensile true strain is defined as $\varepsilon = \ln(1 + \Delta L/L_0)$ with the displacement $\Delta L = 2U$. Although the geometry and loading as well as the boundary condition are all symmetric to the middle planes $X = L_0/2$ and $Y = t_0/2$, we consider the full size specimen so that less constraint will be imposed on the development of deformation localization and fracture.

The overall response of the tensile sheet is presented in terms of the normalized force F^* and normalized minimum cross-sectional area A^*

$$\begin{aligned} F^* &= \frac{F}{\sigma_y^{\text{core}}\bar{t}_0 + \sigma_y^{\text{clad}}(t_0 - \bar{t}_0)} \\ A^* &= \frac{A_{\min}}{A_0} = \frac{t_{\min}}{t_0} \end{aligned} \tag{9}$$

where F is the applied force, and σ_y^{core} and σ_y^{clad} are the yield stresses of the core and clad materials, respectively. The ductility of the sheet is measured in terms of the fracture strain

$$\varepsilon_f = \ln\left(\frac{A_0}{A_f} \right) \tag{10}$$

where A_0 is the original cross-sectional area and A_f is the final cross-sectional area at the neck. The gain in ductility ε_f^* due to cladding is defined as a function of the cladding thickness/volume fraction Γ

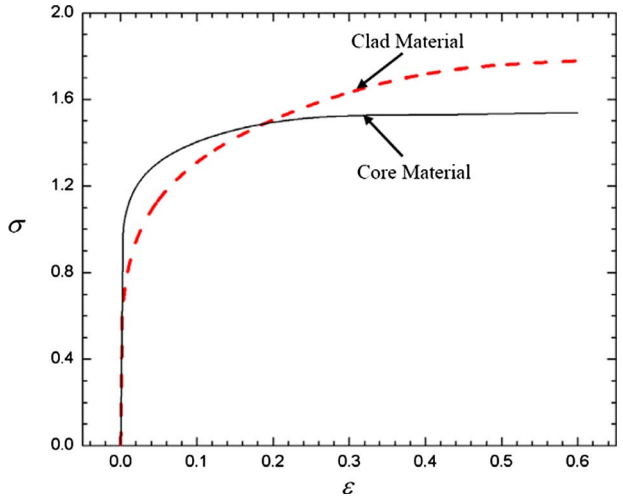

Fig. 2 Uniaxial tension stress and strain curves of the core and clad materials. Stresses are normalized by the yield stress of the core material.

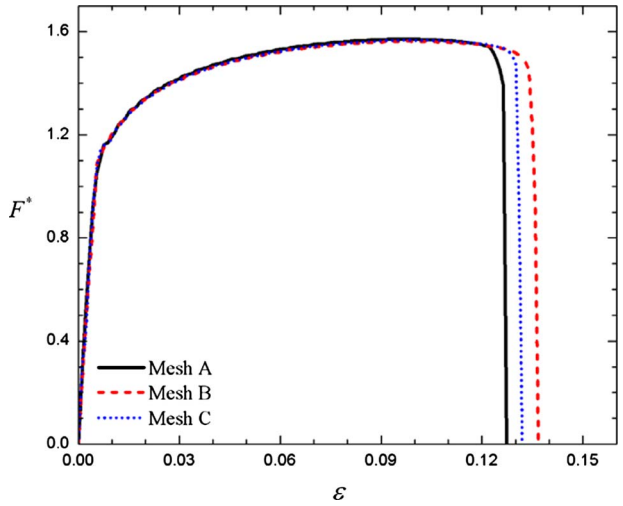

Fig. 4 Predicted normalized force F^* and tensile strain $\varepsilon = \ln(1+U/L_0)$ curve for a monolayer sheet of the core material ($\Gamma=0$)

$$\varepsilon_f^*(\Gamma) = \frac{\varepsilon_f(\Gamma) - \varepsilon_f(0)}{\varepsilon_f(0)} \tag{11}$$

4 Results and Discussions

The elastic-plastic properties of the matrix material of the core layer are specified by $\sigma_y/E=0.0033$, $\nu=0.3$, and $n=10$. We assume that there are no initial voids, and the parameters $q_1=1.0$ and $q_2=1.5$ are used in the yield function (1). The void nucleation is assumed to be plastic strain controlled, with volume fraction $f_N=0.04$ of void nucleating particles, mean strain for nucleation $\varepsilon_N=0.3$, and corresponding standard deviation $s_N=0.1$. The final failure is taken to be characterized by the parameters $f_c=0.15$ and $f_f=0.25$. These values of mechanical properties for the core material are taken from Ref. [15]. The values of the material parameters for the soft cladding layer are assumed to be the same as those for the core except $\sigma_y/E=0.0020$, $n=5$, and $\varepsilon_N=0.5$. This is motivated by the fact that comparing to a core material, a clad material has relatively lower yielding stress but higher hardening and higher resistance to void nucleation. Figure 2 shows the true stress and true strain curves of the core and clad materials under homogeneous uniaxial tension. It is noted that the flow stresses plotted in Fig. 2 are normalized by the yield stress of the core material. In the present paper, we consider a rather stubby specimen with $L_0/t_0=3$, since we are only interested in the neck region. The applied velocity $\dot{U}$ is assumed to be $\dot{U}/L_0=3.33\times10^{-4}$ s^{-1}.

Figure 3 shows a mesh (mesh A) with local refinement around the middle plane $X=L_0/2$, and with a total of 90×60 quadrilateral elements (90 in the X-direction and 60 in the Y-direction), each built up with four linear triangular elements (CPE3 in ABAQUS/EXPLICIT). The element aspect ratio, which is the element size in the Y-direction to the element size in the X-direction, in the local refined area near the middle plane is 2. It is important to point out that the refinement region around the middle plane is identified to fully cover the area where necking and fracture occur. Since deformation localization and fracture depend sensitively on not only the number of elements but also the element aspect ratio [20], mesh B, with 110×60 quadrilateral elements and with the element aspect ratio being 2.5, is designed. A much finer mesh (mesh C), consisting of 140×80 quadrilateral elements with element aspect ratio in the local refinement being 2.5, is also used.

We first consider an extreme case: a metal sheet without cladding ($\Gamma=0\%$ or $\bar{t}_0=t_0$). Figures 4 and 5 present the normalized tensile force F^* and minimum cross-sectional area A^* as functions of the tensile true strain $\varepsilon=\ln(1+U/L_0)$, for the tensile sheet with core layer only ($\Gamma=0\%$). It is found that the force increases linearly with the imposed straining when the deformation is very small and the material is essentially in the elastic state. With continued straining, the force gradually reaches its maximum at around $\varepsilon=0.1$ and then gradually decreases due to both the reduc-

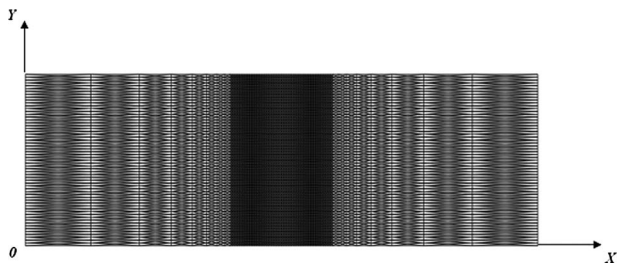

Fig. 3 Mesh A with 90×60 quadrilateral elements (90 in the X-direction and 60 in the Y-direction), each built up with four linear triangular elements (CPE3 in ABAQUS/EXPLICIT)

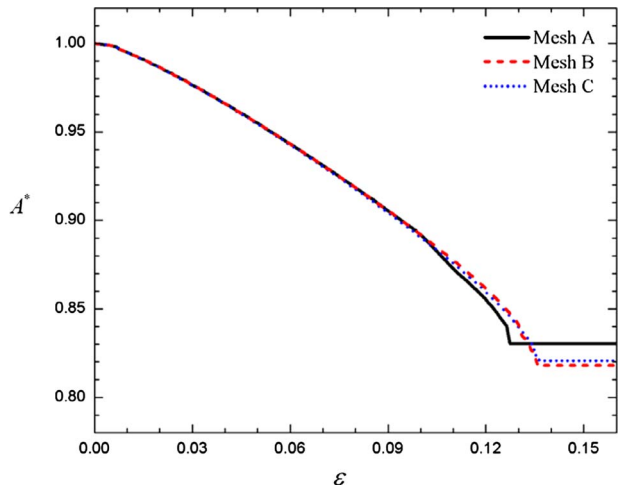

Fig. 5 Predicted normalized minimum cross-sectional area A^* and tensile strain $\varepsilon=\ln(1+U/L_0)$ curve for the monolayer sheet of the core material ($\Gamma=0$)

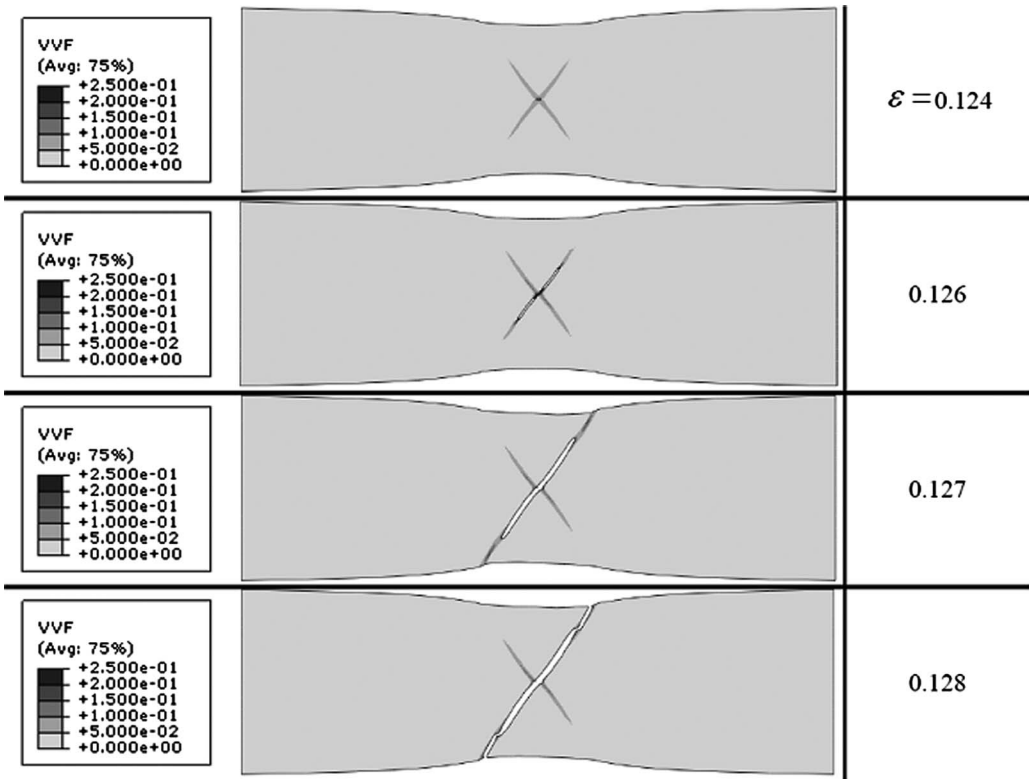

Fig. 6 Predicted distributions of void volume fracture *f* at various deformation stages for the monolayer of the core material ($\Gamma=0$) based on mesh A

tion in the cross-sectional area and the softening effect resulting from void nucleation and growth. Further straining results in a sharp "knee" on the F^* and ε curve, which is associated with reaching the critical value of the void volume fraction ($f_c=0.15$) in the center of the neck. Immediately after the sharp knee, the burst of void nucleation and growth leads to a rapid drop in the true stress, which, in turn, results in a rapid loss of load carry capacity for the tensile sheet. From Fig. 4, it is clear that all the meshes predict quite similar necking and fracture processes. The development of failure process can be more evidently presented in terms of the minimum cross section area $A_{\min}$ versus tensile strain ε (Fig. 5). It is interesting to note that when fracture occurs, neck development essentially stops ($t_{\min}$ is almost a constant). This implies that the reduction in the area at fracture is a representative measure of the onset of macroscopic fracture in the tensile test (see also Ref. [15]). It is interesting to note that necking and failure based on the crude mesh (mesh A) occur earlier than those in the finer meshes (meshes B and C), which is opposite to what one could usually expect. This implies that the element aspect ratio in the critical deformation region is very important in a numerical simulation involved deformation localization and fracture.

Figure 6 shows the predicted distributions of the void volume fraction f at various deformation stages under plane strain tension of the tensile sheet without cladding. It is found that two crossed shear bands, symmetric to the middle plane $X=L_0/2$, are developed after onset of necking at $\varepsilon=0.1$. Fracture initiates at the center of the neck, where the two shear bands cross each other, and where the maximum stress triaxiality ($T=\sigma_H/\sigma_e$) is expected to occur. Due to the initial symmetry, it is expected that cracks will be developed and propagated toward to the top $Y=+t_0/2$ and bottom $Y=-t_0/2$ surfaces along the crossed shear bands. However, the initial geometric symmetry cannot be retained. Instead, the simulations result in a nonsymmetric solution with a single crack as it dissipates less energy. The selection of the single crack is, however, due to numerical round-off errors, which are sensitive to the mesh used.

Significant mesh sensitivity is often expected in a numerical simulation involving fracture. Figure 7 presents the predicted fracture modes based on different meshes. It is important to be noted that the crack patterns shown in Fig. 7 are planar. This planar type

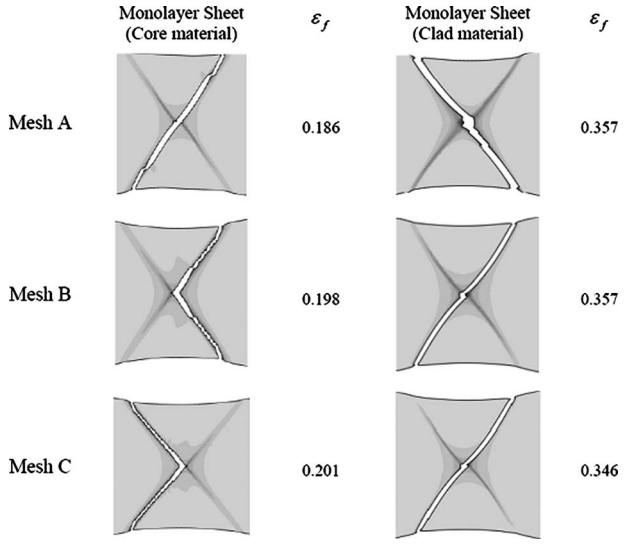

Fig. 7 Predicted fracture modes for monolayer sheets of the core material ($\Gamma=0$) and clad material ($\Gamma=100\%$) based on the different meshes

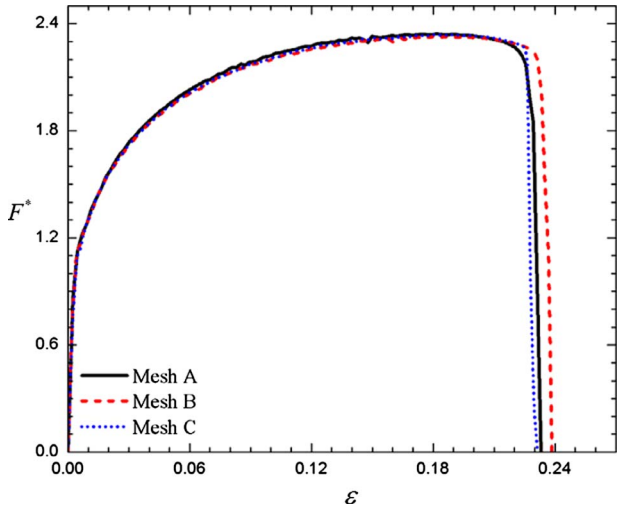

Fig. 8 Predicted normalized force F^* and tensile strain $\varepsilon = \ln(1+U/L_0)$ curve for a monolayer sheet of the clad material ($\Gamma = 100\%$)

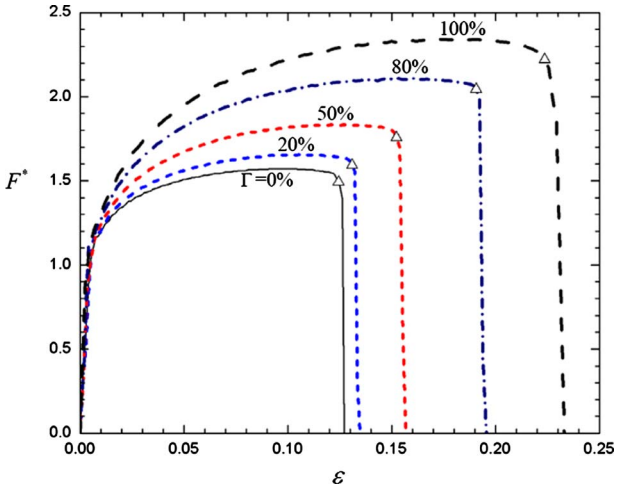

Fig. 10 Predicted normalized force F^* and tensile strain $\varepsilon = \ln(1+U/L_0)$ curves for tensile sheets with various cladding thickness ratio Γ. Open triangles indicate the initiation of cracking.

of fracture surface is identical in appearance to that of the cone portion of the cup-cone fracture of ductile tensile test specimens of circular cross section [21]. This fracture mechanism corresponds to the void-sheet mechanism of the shear fracture. It is also important to be noted that the double-cup fracture mode is more commonly observed in ductile sheet metal tensile samples [21,22]. However, in the plane strain tension considered in the present study, the process of void nucleation and growth occurs much earlier than in uniaxial tension. Since by definition the formation of a shear band requires conditions of plane strain, the plane strain samples favor the conditions for void-sheet mechanism of the shear fracture to occur more readily.

We now consider another extreme: a tensile sheet made entirely of the clad material ($\Gamma = 100\%$ or $\bar{t}_0 = 0$). As mentioned previously, comparing to the core material, the clad material has relatively lower yielding stress but higher hardening (Fig. 2). It is expected that the process of necking and cracking in the tensile sheet of the clad material will be noticeably delayed compared with that in the tensile sheet made of the core material. Figures 8 and 9 show the normalized tensile force F^* and minimum cross-sectional area A^* as functions of the tensile true strain $\varepsilon = \ln(1+U/L_0)$, for the monolayer sheet ($\Gamma = 100\%$). It is observed that all the meshes predict very close overall tensile responses in terms of the applied force and minimum cross-sectional area. The predicted fracture surfaces are again planar (Fig. 7). Since the typical crack patterns, observed experimentally in monolayer metal sheets under tension, can be numerically reproduced by either mesh A or mesh C, both meshes will be used in the rest of the present paper. Meshes A and C together should be sufficient to assess the effects of cladding on fracture although they are still crude in relation to the crack tip field. However, some figures are presented by using the numerical results based on mesh A only if the difference in the numerical results between meshes A and C is small enough.

We proceed by studying the effects of cladding on fracture in sheet metals under plane strain tension. Figures 10 and 11 show the normalized force F^* and the minimum cross-sectional, area A^* versus the tensile strain ε curves, respectively. It is observed that cladding a ductile soft layer increases the strain at which the applied force reaches its maximum. This implies that cladding increases the strain to necking. It is also found from Figs. 10 and 11 that cladding delays cracking (open triangles indicate the initiation of cracking). Furthermore, from Fig. 11, the maximum reduction in area, indicated by the constant A^* lines, increases with increas-

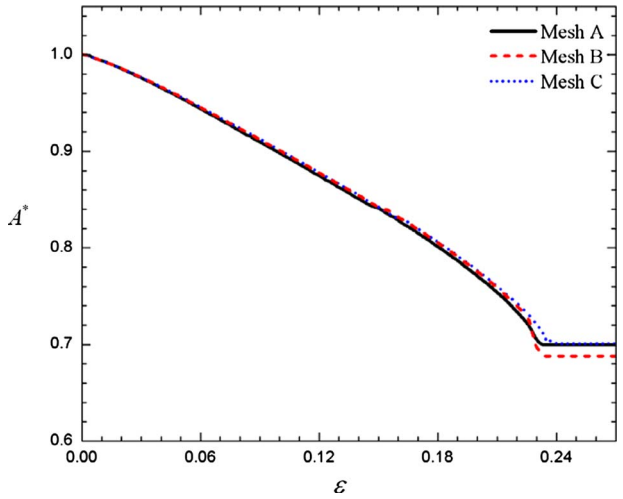

Fig. 9 Predicted normalized minimum cross-sectional area A^* and tensile strain $\varepsilon = \ln(1+U/L_0)$ curve for the monolayer sheet of the clad material ($\Gamma = 100\%$)

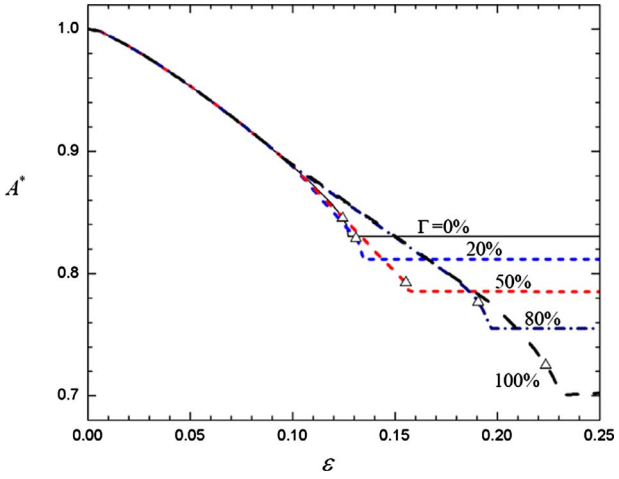

Fig. 11 Predicted normalized minimum cross-sectional area A^* and tensile strain $\varepsilon = \ln(1+U/L_0)$ curves for tensile sheets with various cladding thickness ratio Γ. Open triangles indicate the initiation of cracking.

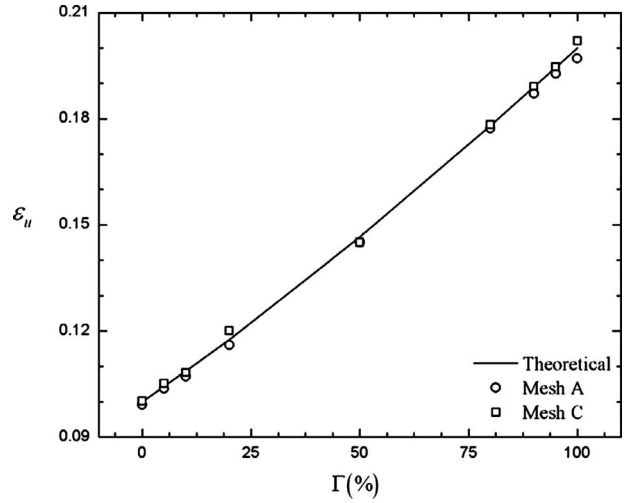

Fig. 12 Predicted strain to necking ε_u for tensile sheets with various cladding thickness percentages Γ

ing cladding. This means that the ductility is enhanced by cladding.

The predicted effect of cladding on necking is more clearly shown in Fig. 12. Numerical results indicate that the predicted necking strain is not sensitive to the meshes used. Figure 12 also includes the necking strains based on the Considère-type criterion $d\bar{\sigma}_a/d\bar{\varepsilon}=\bar{\sigma}_a$. Here, the averaged flow stress $\bar{\sigma}_a$ for the laminated sheet is calculated from the mixture rule $\bar{\sigma}_a=(1-\Gamma)\bar{\sigma}_{core}+\Gamma\bar{\sigma}_{clad}$, where $\bar{\sigma}_{core}$ and $\bar{\sigma}_{clad}$ are the flow stresses for the core and cladding layer, respectively [1]. The excellent agreement between the theoretical prediction and numerical simulations indicates that the overall hardening behavior of a layered structure can be described well with the rule of mixtures, and that significant void growth has not occurred prior to necking. However, it has been generally accepted that fracture in layered structures does not follow the mixture rule [23,1].

Figures 13 and 14 show the predicted fracture processes in tensile sheets with various cladding thickness ratio Γ based on meshes A and C, respectively. It is found that in monolayer sheets (Γ=0%, 100%), crack initiates at the center of the specimen and propagates toward both top and bottom surfaces along the dominated shear band. In bilayer sheets with $\Gamma \leq 50\%$, crack occurs in the core material close to the interface. The initiated crack first propagates in two directions along the dominated shear band until it goes through the whole core layer and then further runs into the clad layer until the specimen is fully fractured. When the cladding layer is noticeably thicker than the core, for example Γ=80%, crack initiates either in the clad nearby the center of the specimen or in the core. However, the initiated crack always first runs through the whole core layer and then propagates through the clad layer.

Figure 15 presents the predicted gain in fracture strain ε_f^*, defined in Eq. (11), in sheet metals with various cladding volume fractions Γ. It is observed that the increase in fracture strain is a nonlinear function of the cladding volume fraction Γ.

Finally, we would like to emphasize that the numerical results depend sensitively on the mechanical properties of both core and clad materials. Our parametrical study has indicated that, though not reported in the present paper, increasing hardening $1/n$, mean strain for nucleation ε_N, and void volume fractions at coalescence f_c and at fracture f_f delays necking and enhances ductility. Numerical results are also sensitive to the clad ratio Γ and the difference in the mechanical properties between the core and clad layer. In the present paper, the selection of the values of the material parameters has been motivated by the fact that comparing to a core material, a clad material has relatively lower yielding stress

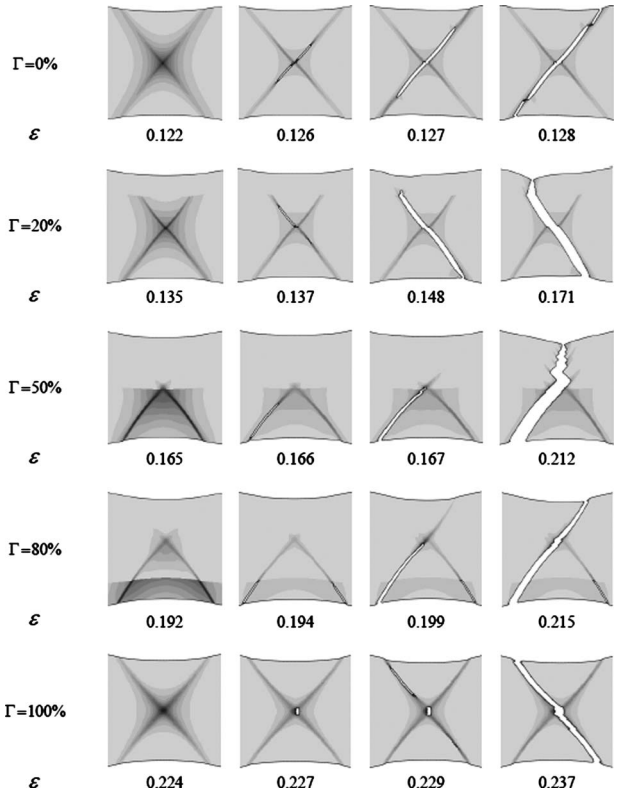

Fig. 13 Predicted fracture processes for tensile sheets with various cladding thickness percentages Γ based on mesh A

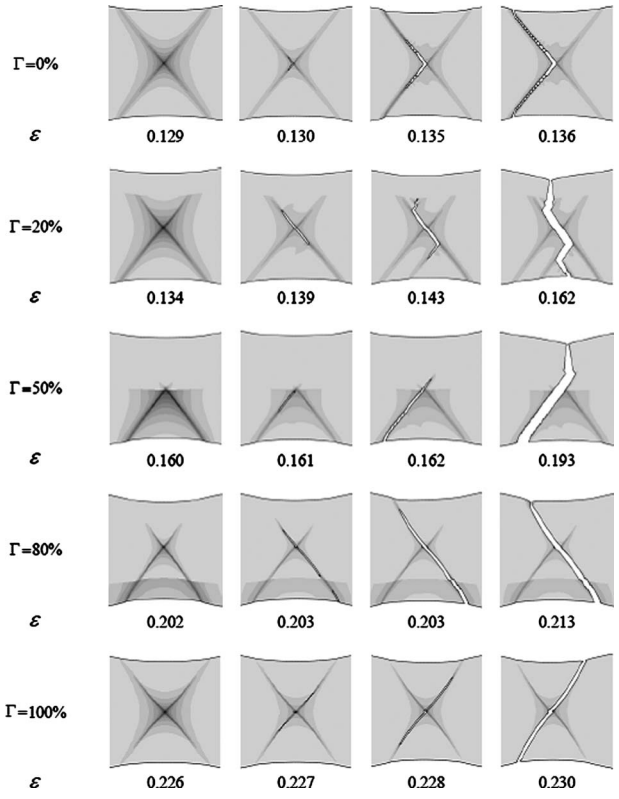

Fig. 14 Predicted fracture processes for tensile sheets with various cladding thickness percentages Γ based on mesh C

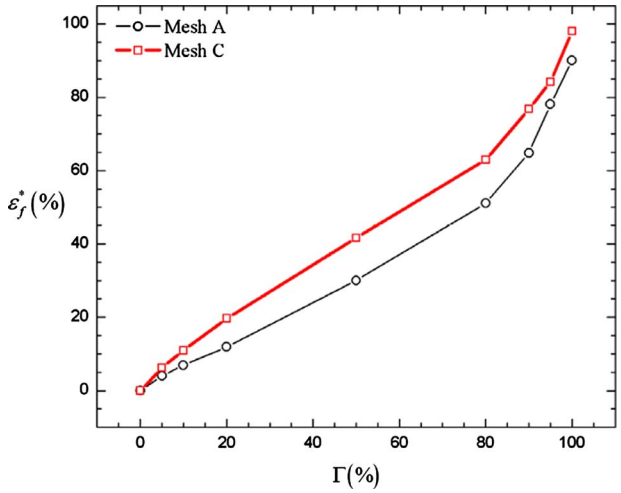

Fig. 15 Predicted normalized fracture strain ε_f^* in tensile sheets with various cladding thickness ratios Γ

but higher hardening and higher resistance to void nucleation. This assumption seems to be appropriate in view of practical applications.

5 Conclusions

We have carried out a finite element analysis of effects of cladding on necking and fracture in tensile sheet metals. It has been demonstrated that cladding a ductile soft layer increases both the necking strain (Fig. 12) and fracture strain (Fig. 15). The increase in the necking strain has been found to be due to the fact that cladding a ductile layer enhances the overall work hardening for the layered metal sheets according to the rule of mixtures. Furthermore, the increase in the necking strain slows down the development of the triaxial tensile stress inside the neck, which delays the void nucleation and growth, and which, in turn, contributes to enhancement in ductility. It should be pointed out that the calculated subtle change in the appearance of the fracture surface due to cladding is very sensitive to the mesh used (Figs. 13 and 14).

While we have studied the effect of cladding on fracture in sheet metals under stretching, experimental work has shown that cladding significantly increases the bendability in sheet metals [10]. Numerical simulations of the effect of cladding on bendability are in progress and will be reported elsewhere.

Acknowledgment

This work is supported by the Natural Sciences and Engineering Research Council of Canada (NSERC), Ontario Centre of Excellence (OCE), and Novelis Global Technology Centre.

References

[1] Lesuer, D. R., Syn, C. K., Sherby, O. D., Wadsworth, J., Lewandowski, J. J., and Hunt, W. H., Jr., 1996, "Mechanical Behaviour of Laminated Metal Composites," Int. Mater. Rev., **41**, pp. 169–197.
[2] Manoharan, M., Ellis, L., and Lewandowski, J. J., 1990, "Laminated Composites With Improved Toughness," Scr. Metall. Mater., **24**, pp. 1515–1519.
[3] Ritchie, R. O., 1988, "Mechanisms of Fatigue Crack-Propagation in Metals, Ceramics and Composites—Role of Crack Tip Shielding," Mater. Sci. Eng., A, **103**, pp. 15–28.
[4] Kum, D. W., Oyama, T., Wadsworth, J., and Sherby, O. D., 1983, "The Impact Properties of Laminated Composites Containing Ultrahigh Carbon (UHC) Steels," J. Mech. Phys. Solids, **31**, pp. 173–186.
[5] Kim, K. J., Kim, D., Choi, S. H., Chung, K., Shin, K. S., Barlat, F., Oh, K. H., and Youn, J. R., 2003, "Formability of AA5182/Polypropylene/AA5182 Sandwich Sheets," J. Mater. Process. Technol., **139**, pp. 1–7.
[6] Li, T., and Suo, Z., 2006, "Deformability of Thin Metal Films on Elastomer Substrates," Int. J. Solids Struct., **43**, pp. 2351–2363.
[7] Xue, Z., and Hutchinson, J. W., 2007, "Neck Retardation and Enhanced Energy Absorption in Metal-Elastomer Bilayers," Mech. Mater., **39**, pp. 473–487.
[8] Semiatin, S. L., and Piehler, H. R., 1979, "Formability of Sandwich Sheet Materials in Plane Strain Compression and Rolling," Metall. Trans. A, **10A**, pp. 97–107.
[9] Chen, A. Y., Zhang, J. B., Lu, J., Lun, W., and Song, H. W., 2007, "Necking Propagated Deformation Behaviour of Layer-Structured Steel Prepared by Co-Warm Rolled Surface Nanocrystallized 304 Stainless Steel," Mater. Lett., **61**, pp. 5191–5193.
[10] Wagstaff, R. B., Lloyd, D. J., and Bischoff, T. F., 2006, "Direct Chill Casting of CLAD Ingot," Mater. Sci. Forum, **519–521**, pp. 1809–1814.
[11] Gurson, A. L., 1977, "Continuum Theory of Ductile Rupture by Void Nucleation and Growth. Part I—Yield Criteria and Flow Rules for Porous Ductile Media," ASME J. Eng. Mater. Technol., **99**, pp. 2–15.
[12] Tvergaard, V., 1989, "Material Failure by Void Growth to Coalescence," Adv. Appl. Mech., **27**, pp. 83–151.
[13] Tvergaard, V., 1981, "Influence of Voids on Shear Band Instabilities Under Plane Strain Conditions," Int. J. Fract., **17**, pp. 389–407.
[14] Tvergaard, V., 1982, "On Localization in Ductile Materials Containing Spherical Voids," Int. J. Fract., **18**, pp. 237–252.
[15] Tvergaard, V., and Needleman, A., 1984, "Analysis of the Cup-Cone Fracture in a Round Tensile Bar," Acta Metall., **32**, pp. 157–169.
[16] Chu, C. C., and Needleman, A., 1980, "Void Nucleation Effects in Biaxially Stretched Sheets," ASME J. Eng. Mater. Technol., **102**, pp. 249–256.
[17] Mear, M. E., and Hutchinson, J. W., 1985, "Influence of Yield Surface Curvature on Flow Localization in Dilatants Plasticity," Mech. Mater., **4**, pp. 395–407.
[18] Chen, B., Huang, Y., Liu, C., Wu, P. D., and MacEwen, S. R., 2004, "A Dilatational Plasticity Theory for Viscoplastic Materials," Mech. Mater., **36**, pp. 679–689.
[19] Nahshon, K., and Hutchinson, J. W., 2008, "Modification of the Gurson Model for Shear Failure," Eur. J. Mech. A/Solids, **27**, pp. 1–17.
[20] Besson, J., Steglich, D., and Brocks, W., 2001, "Modeling of Crack Growth in Round Bars and Plane Strain Specimens," Int. J. Solids Struct., **38**, pp. 8259–8284.
[21] Weinrich, P. F., and French, I. E., 1976, "The Influence of Hydrostatic Pressure on the Fracture Mechanisms of Sheet Tensile Specimens of Copper and Brass," Acta Metall., **24**, pp. 317–322.
[22] Gimple, J. L., Wilkinson, D. S., Embury, J. D., and Lewandowski, J. J., 2001, "Effect of Superimposed Pressure on the Fracture Behaviour of Aluminum Automotive Alloys," *Proceedings of the TMS Aluminum 2001*, S. K. Das, J. G. Kaufman, and T. J. Lienert, eds., TMS, Indianapolis, IN, pp. 17–29.
[23] Semiatin, S. L., and Piehler, H. R., 1979, "Deformation of Sandwich Sheet Materials in Uniaxial Tension," Metall. Mater. Trans. A, **10**, pp. 85–96.